Journal of Alloys and Compounds 504 (2010) 237–242

Contents lists available at ScienceDirect

Journal of Alloys and Compounds

journal homepage: www.elsevier.com/locate/jallcom

Effect of heat treatment on corrosion properties of sol–gel titania–ceria nanocomposite coating

A. Ghasemi, T. Shahrabi*, A.A. Oskuie, H. Hasannejad, S. Sanjabi

Materials Engineering Department, Faculty of Engineering, Tarbiat Modares University, P.O. Box 14115-143, Tehran, Iran

ARTICLE INFO

Article history:
Received 5 April 2010
Received in revised form 11 May 2010
Accepted 21 May 2010
Available online 31 May 2010

Keywords:
Titanium oxide
Cerium oxide
Coating materials
Heat treatment
Corrosion
Sol–gel

ABSTRACT

The objective of this work is to study the effect of heat treatment temperature on corrosion resistance of TiO_2–CeO_2 composite coatings deposited by sol–gel method. TiO_2–CeO_2 thin films were applied on 316L stainless steel substrates via spin coating technique. The samples were heat treated at different temperatures from 300 to 500 °C and the corrosion resistance of the coated samples was determined by dynamic polarization and electrochemical impedance spectroscopy (EIS) studies. Microstructures of the films were characterized by scanning electron microscopy (SEM), energy dispersive X-ray analyses (EDX), X-ray diffraction (XRD), and differential thermal analysis (DTA). The results obtained from corrosion data showed that TiO_2–CeO_2 coating improves the corrosion resistance of 316L stainless steel substrate and higher pitting resistance achieved in comparison with the bare samples. On the other hand, corrosion current densities of the samples increased for more than three times as higher heat treatment temperatures were exploited.

1. Introduction

In spite of good corrosion properties of stainless steels, they still tend to corrode in the presence of halide ions [1]. One of the most effective methods to tackle this problem is to coat the surface of stainless steel with protective ceramic compounds such as transition metal oxides, nitrides, carbides or silicates [2]. Among ceramics, oxide coatings have excellent chemical stability and there are many reports in the literature of their beneficial effects on corrosion resistance [3,4].

TiO_2 coatings have gained attention recently due to their photocatalytic properties and their ability to free electron when they are exposed to light [5]. TiO_2 is an n-type semiconductor and an ultraviolet (UV) light sensitive material [6]. Furthermore, TiO_2 has excellent chemical stability, heat resistance and low electron conductivity, making it a corrosion proof material [7]. Recently, the application of the TiO_2 coating for cathodic protection of metals under UV illumination has been reported in the literature [4]. However, the protection mechanism of such a coating suggests that they are only suitable when their surface is intact. Small defects undermine their integrity and protective properties [8]. Many attempts have been made to modify TiO_2 coatings by doping of metallic and nonmetallic ions [9]. Incorporation of other components to the coating is another solution to overcome the limitation of single component oxide layers and improve their protection [4]. Being a well known corrosion inhibitor, CeO_2 seems to be a promising choice to be incorporated into oxide films to form a composite coating [9].

Widely used sol–gel process offers numerous advantages over other conventional deposition techniques, including the ability to tailor film properties, low cost and possibility of processing at low temperatures [10,11]. Sol–gel protective coatings have shown excellent chemical stability, oxidation mitigation and enhanced corrosion resistance in various corrosive mediums and are practically applied on metal substrates [1].

In this work, the effect of heat treatment temperature on electrochemical, structural and corrosion properties of sol–gel TiO_2–CeO_2 composite films applied by spin coating method was studied.

2. Experimental procedure

2.1. Sol preparation

Titanium oxide sol is prepared by mixing ceric ammonium nitrate and titanium butoxide to get the molar ratio of 1:10 between Ce:Ti in ethanol. The mixture stirred vigorously at room temperature for 30 min. In the next step, small amount of distilled water was added to the mixture to accelerate hydrolysis and condensation. Then the suspension stirred for 10 h until it turns to a clear solution. In order to obtain a Ce^{2+} rich solution, the prepared TiO_2–CeO_2 sol was aged for 8 days at room temperature with humidity of (50 ± 5%). Within a few days, the color of the solution changed from deep red to pale yellow, indicating a reduction of Ce^{4+} by ethanol.

Fig. 1 describes the flow diagram for preparation of TiO_2–CeO_2 sol, followed by its deposition on 316L stainless steel substrates by spin coating.

* Corresponding author. Tel.: +98 21 82883378; fax: +98 21 88005040.
E-mail addresses: tshahrabi34@modares.ac.ir (T. Shahrabi), a.oskuie@modares.ac.ir (A.A. Oskuie).

0925-8388/$ – see front matter © 2010 Elsevier B.V. All rights reserved.
doi:10.1016/j.jallcom.2010.05.100

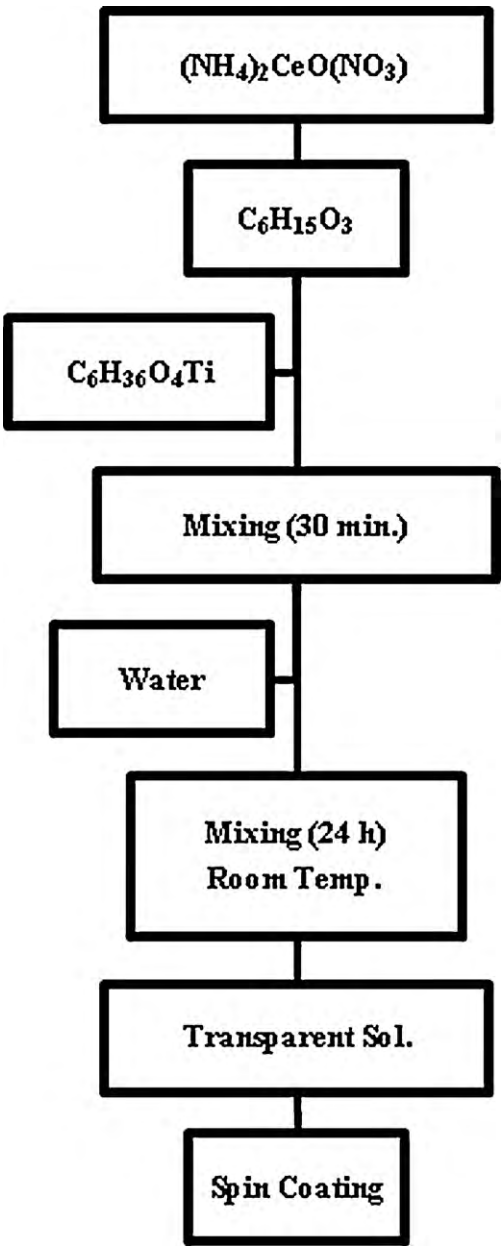

Fig. 1. Flow diagram of TiO_2–CeO_2 coating process by the sol–gel method.

2.2. Substrates and coatings

316L stainless steel rolled plates (containing approximately 18% nickel, 8% chromium, 2% molybdenum and less than 0.003% carbon produced by Jiangyin Xingye Stainless Steel Co.) with thickness of 3 mm were used as substrate. Samples, cut to a size of 1 cm × 2 cm, were ground with emery papers 320–1500 grit size followed by mirror polishing with 0.3 μm Al_2O_3 powder, and finally the specimens were cleaned in acetone with ultrasonic cleaner for 10 min.

The TiO_2–CeO_2 composite films were deposited on 316L stainless steel substrates using spin coater (Model: TC100, MTI corporation, USA) at spinning rate of 3000 rpm. Then the samples were dried for 1 h at 100 °C. The samples were coated and dried for three times. The coated specimens were heat treated inside a muffle furnace at different temperatures of 300, 400, and 500 °C for 1 h in atmospheric condition. Heating and cooling rate were adjusted at 60 °C/h.

2.3. Microstructural and compositional analysis

X-ray diffraction analyses (XRD, model XPert, Philips) under CuK_α was used to analyze the structure and phases present in the TiO_2–CeO_2 composite films deposited on 316L stainless steel substrates. The morphology and the composition of the coatings were examined using Scanning electron microscopy (SEM) and energy dispersive X-ray (EDX) spectroscopy (model Vega, manufacture Tescan). Differential thermal analysis (DTA, model STA 429, Netzsch Thermoanalyse) was performed on a dried sample. All analyses were executed in aerated atmosphere at heating rate of 10 °C/min up to 500 °C using alumina as the reference material.

2.4. Electrochemical measurements

Electrochemical parameters of the TiO_2–CeO_2 coated 316L stainless steel samples were determined by potentiodynamic polarization curves and electrochemical impedance spectroscopy (EIS) using a computer controlled potentiostat/galvanostat (EG&G Prinston Applied Research, 273A).

All electrochemical tests (potentiodynamic polarization and the EIS) were carried out in a conventional three electrode electrochemical cell (a saturated calomel electrode as the reference electrode, a platinum plate as the counter and the coated samples as the working electrodes) in an aerated 3.5% NaCl solution at room temperature. To reach a constant open circuit potential (E_{OCP}), the samples were in the solution for 1 h before starting the tests. Each electrochemical test was repeated two times to ensure the reliability of the data.

Potential scan rates for polarization studies were fixed at 0.6 mV/s. All potential scans were carried out in a potential range from −150 mV (cathodic) to +1200 mV (anodic) relative to the OCP. The impedance measurements were conducted using a PowerSuite software analyzer in a frequency range of 10 mHz to 100 kHz at the OCP by applying a sinusoidal potential wave with a 10 mV amplitude. The computer system was equipped with a PowerSuite software analyzer for recording EIS data and Zview program to determine the values of the parameters of the proposed electric circuit model. The impedance data were curve fitted and the pertinent (EIS) parameters were extracted using Zview program.

3. Results and discussion

3.1. Microstructural characterization

Fig. 2 shows X-ray diffraction patterns of TiO_2–CeO_2 composite coatings that were heat treated at three different temperatures (i.e. 300, 400, and 500 °C). It can be found from Fig. 2 that the structure of titania–ceria composite coating gradually changed from a totally amorphous structure at 300 °C to a crystalline structure at 500 °C.

X-ray pattern obtained from the sample heat treated at 500 °C indicates the presence of CeO_2 (cerianite) phase with peaks corresponding to (1 1 1), (2 0 0), (2 2 0) and (3 1 1) planes. The absence of TiO_2 characteristic peaks implies that the crystalline CeO_2 phase is dispersed in amorphous titanium oxide. The crystallite size was

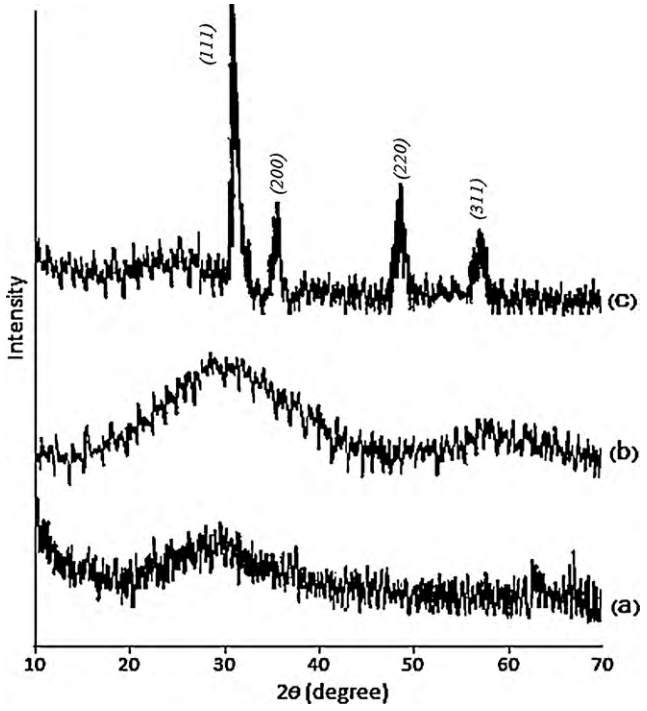

Fig. 2. X-ray diffraction patterns of sol–gel derived TiO_2–CeO_2 composite films heat treated at (a) 300 °C, (b) 400 °C, and (c) 500 °C.

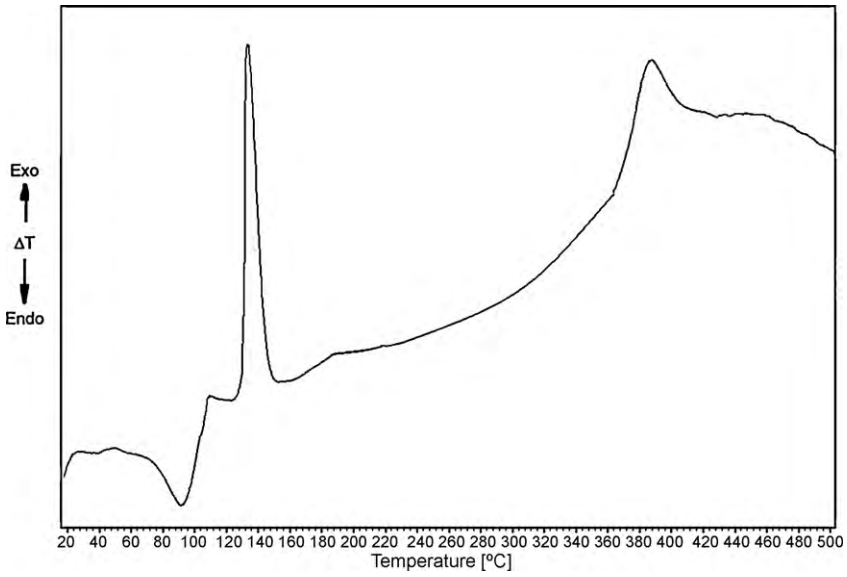

Fig. 3. DTA pattern of dried TiO_2–CeO_2 gel (heating rate: 10 °C min^{-1}, air atmosphere).

determined using Scherer's equation as:

$$d_{h\,kl} = \frac{0.89\lambda}{\beta \times \mathrm{Cos}\,2\theta} \quad (1)$$

where d_{hkl} denotes the average crystallite size, λ the X-ray wavelength of CuKα (here 0.154 nm), β the full width of the peak measured at half maximum intensity (FWHM) and θ is the Bragg's angle of the peak [12]. The calculation of crystallite size using the Scherer's equation estimated the crystallite size of the coating heat treated at 500 °C to be 22 nm.

DTA result from heating the dried sample of TiO_2–CeO_2 sol from room temperature to 500 °C is presented in Fig. 3. Three obvious peaks are distinguishable in this figure. The first endothermic peak is positioned about 100 °C which is related to the release of solvent or physisorbed and chemisorbed water contained in the dried sample [12]. Following this endotherm peak there are two other exothermic peaks at 130 and 390 °C. The former is attributed to the combustion of the organic matter of the precursors [12] and the latter is the result of cerianite crystallization [13], which is also corroborated by the X-ray diffraction patterns.

SEM micrographs of the TiO_2–CeO_2 composite coatings on 316L stainless steel and heat treated at different temperatures are depicted in Fig. 4. Morphologies observed in this figure are quite homogeneous and free from defects such as micro-cracks. With increasing the heat treatment temperature even up to 500 °C no such detectable flaws appear in the coatings. The integrity of the coating observed in the SEM images for samples heat treated at different temperatures have direct bearing on the electrochemical properties and consequently corrosion properties of the films. The result of EDX analysis is shown in Fig. 5. The peaks of Ti and Ce, which are a clue to the presence of TiO_2 and CeO_2 in the coating, are accompanied with Fe, Cr and Ni peaks which were detected from the stainless substrates.

3.2. Electrochemical measurements

Potentiodynamic curves of TiO_2–CeO_2 composite films deposited on 316L stainless steel substrates and sintered at 300, 400 and 500 °C are given in Fig. 6. Comparison of these curves reveals that by application of TiO_2–CeO_2 composite films on stainless steel substrates the potentiodynamic curves were shifted to the left (lower corrosion current density) and more negative potentials with respect to the uncoated samples. Bethencourt et al. [14] reported before that the inhibition mechanism of cerium is cathodic so this behavior was predictable.

Values of corrosion potential (E_{corr}), corrosion current density (i_{corr}), pitting potential (E_{pit}), passivity region span ($E_{pit} - E_{corr}$) and corrosion rates of TiO_2–CeO_2 composite films sintered at different temperatures are reported in Table 1.

According to Table 1, the uncoated 316L stainless steel possessed the highest corrosion current density (i_{corr} = 21.6 μA/cm^2). Application of TiO_2–CeO_2 composite coating on stainless steel substrates substantially decreased the corrosion current density in the saline solution. It suggests that TiO_2–CeO_2 coated 316L stainless steels were more corrosion resistant than uncoated ones. The trend of reported corrosion potentials in Table 1 reveals that the lower the sintering temperature, the more negative is the corrosion potential (E_{corr}), which is desirable in terms of corrosion resistance. Corrosion current density and thus corrosion rate also concurrently decline with this negative shift of corrosion potential with decreasing the sintering temperature. All of these results demonstrated that heat treating the samples at higher temperatures lowered the corrosion resistance of the films. Inferior corrosion behavior of the coated samples heat treated at 500 °C can be explained by the crystallization of CeO_2 which was discussed in previous section. As it was stated, XRD studies pinpointed crystallization of CeO_2 in TiO_2–CeO_2 composite coating crystallization at 500 °C. Partially crystalline TiO_2–CeO_2 composite coatings show less corrosion resistance with respect to amorphous structure which can be attributed to good ion and electron conduction of the crystalline films.

One of the most important properties of 316L stainless steel is its pitting corrosion resistance. Results inferred from the size of passivity region ($E_{pit} - E_{corr}$) also prove superior pitting resistance of TiO_2–CeO_2 coated 316L stainless steels with respect to uncoated one. This behavior of the coated specimens illustrates the role of the TiO_2–CeO_2 composite coating in blocking the active sites and thus mitigating further extension of effective electroactive areas. These results also show that by raising the sintering temperature from 300 to 500 °C, samples become more susceptible to pitting corrosion. Crystallization of CeO_2 in amorphous TiO_2 matrix may explain this behavior. Each phase transition is accompanied by a change in volume and in this case the crystallization of CeO_2 phase in the TiO_2 amorphous matrix might have exerted enough tension to produce fissures in the coating heat treated at 500 °C.

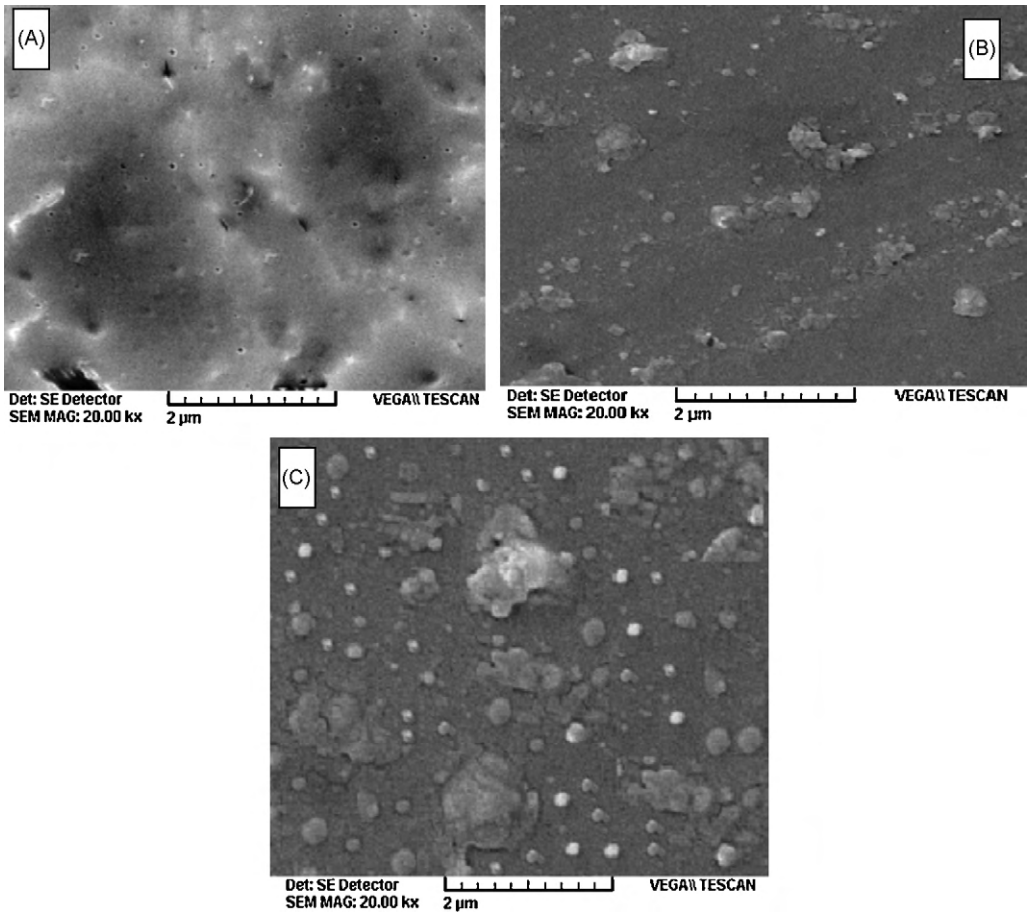

Fig. 4. SEM micrographs of sol–gel derived TiO_2–CeO_2 composite films heat treated at (a) 300 °C, (b) 400 °C, and (c) 500 °C.

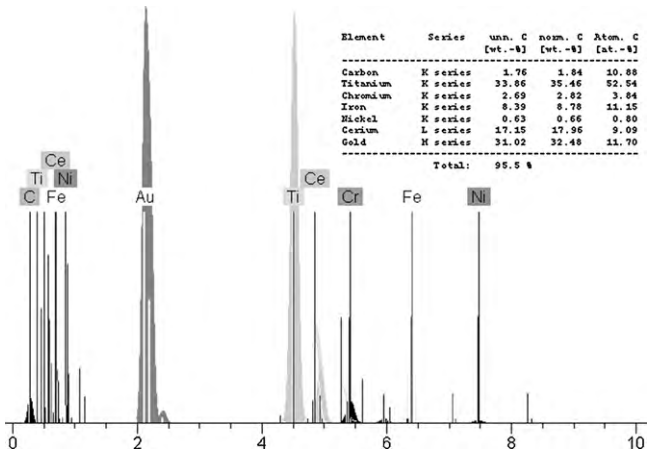

Fig. 5. Energy dispersive X-ray analysis (EDX) of TiO_2–CeO_2 coated 316L stainless steel sample.

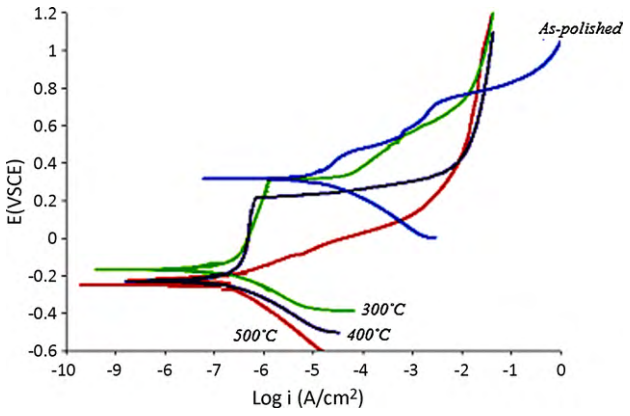

Fig. 6. Potentiodynamic polarization curves for TiO_2–CeO_2 composite films heat treated at 300, 400, and 500 °C in 3.5% NaCl solution.

Table 1
Values of E_{corr}, i_{corr}, E_{pit}, $E_{pit} - E_{corr}$ and corrosion rate measured by potentiodynamic tests (Fig. 6).

T (°C)	i_{corr} (µA/cm^2)	E_{corr} vs. OCP (mV)	E_{pit} (mV)	$E_{pit} - E_{corr}$ (mV)	C.R. (mpy)
As-polished	21.632	+318	+480	162	8.85
300	0.140	−164	+307	471	0.057
400	0.363	−224	+218	442	0.15
500	0.440	−268	−73	195	0.18

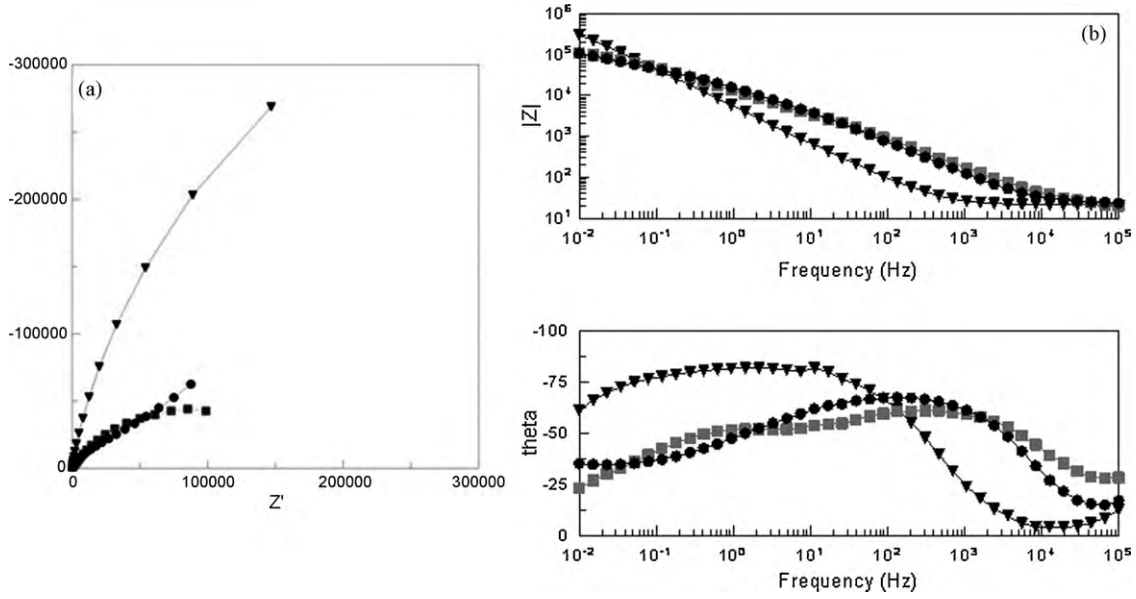

Fig. 7. Nyquist (a) and Bode (b) plots of electrochemical impedance spectra for the TiO_2–CeO_2 composite films heat treated at 300 °C (■), 400 °C (●), and 500 °C (▲) in 3.5% NaCl solution.

Fig. 7 presents Nyquist and Bode plots of the TiO_2–CeO_2 composite films that were sintered at different temperatures in 3.5% NaCl solution. According to EIS measurements (Fig. 7), TiO_2–CeO_2 composite coatings heat treated at 300 °C again showed the best corrosion properties in 3.5 wt% NaCl solution. Based on these results, specimens sintered at 400 and 500 °C respectively ranked after the sample heat treated at 300 °C. As it was discussed before this phenomenon can be due to the fact that amorphous structure obtained at 300 °C has less ionic conductivity and is less defective. Parameters of electrochemical properties of the composite layer were obtained using curve fitting method by Zview software (Fig. 7).

Schematic model of the TiO_2–CeO_2 composite coating and its equivalent electric circuit are presented in Fig. 8. This circuit consists of electrolyte resistance ($R_{solution}$), coating resistance ($R_{sol-gel}$) paralleled with a constant phase element representing sol–gel layers on metal ($CPE_{sol-gel\ layer}$) and coating pore resistance (R_{crack}) paralleled with a constant phase element representing the cerium oxide islands ($CPE_{islands}$). To simulate real conditions constant phase elements (CPE) instead of pure capacitors were introduced in the fitting method. The impedance of a CPE is a function of frequency as follows [15]:

$$Z_{CPE} = \frac{1}{Q(j\omega)^n} \tag{2}$$

where Q represents the frequency independent parameter of constant phase impedance and n defines the extent of deviation from the ideal behavior.

The capacitance can be calculated from the Eq. (3):

$$C = Q(\omega_{max})^{n-1} \tag{3}$$

Here ω_{max} is the frequency of maximum imaginary impedance for a definite time constant. The term Q in the preceding equation is the pseudo capacitance of the system that is defined by Eq. (4):

$$Q = \frac{r\varepsilon\varepsilon_o A}{d} \tag{4}$$

In this equation, ε_o is the permittivity of free space, ε is the dielectric constant of the surface film, d is the thickness of the coating, A is the exposed area and r is the roughness factor.

Values of the circuit parameters obtained by curve fitting are listed in Table 2. Polarization resistance becomes lower with increasing the heat treatment temperature from 300 to 500 °C, as can be seen from Nyquist plot drawn in Fig. 7(a). Based on the EIS measurements, reported in Table 2, resistance of the coating sintered at 300 °C is $8.62 \times 10^7\ \Omega\,cm^2$ but decreased to $6.97 \times 10^6\ \Omega\,cm^2$ when the coating was heat treated at 400 °C and dropped further to $1.93 \times 10^5\ \Omega\,cm^2$ when sintered at 500 °C. This trend emphasizes the effect of crystallization of CeO_2 in amorphous TiO_2 matrix. The capacitance and resistance values of the coating represent its ability to protect the substrates against corrosion. Higher resistance values and lower capacitance values mean better impedance properties [16]. Therefore resistance and capacitance values of the TiO_2–CeO_2 composite films heat treated at 300 °C again confirms the conclusion made in previous section that the coating sintered at 300 °C has the best corrosion resistance.

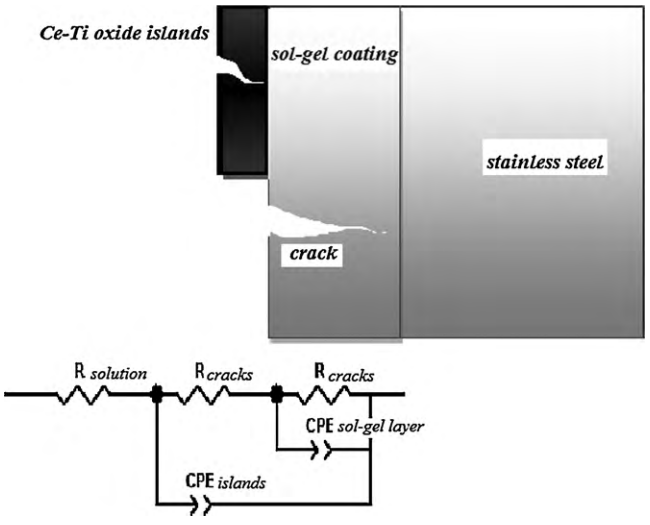

Fig. 8. Schematic representation of sol–gel derived TiO_2–CeO_2 coated stainless steel and Equivalent circuit used to fit the experimental impedance spectra.

Table 2
Fitting parameters for the data given in Fig. 8.

T (°C)	$R_{solution}$ (Ω cm^2)	$R_{islands}$ (Ω cm^2)	$R_{sol-gel}$ (Ω cm^2)	$C_{sol-gel}$ (nF/cm^2)	$n_{sol-gel}$	C_{island} (nF/cm^2)	n_{island}
300	23	9.58	8.62×10^7	3.02×10^{-6}	8.99×10^{-1}	4.50×10^{-6}	8.99×10^{-1}
400	31.18	2.70	6.97×10^6	5.67×10^{-6}	8.10×10^{-1}	2.30×10^{-5}	3.44×10^{-1}
500	12.87	5.35	1.93×10^5	3.90×10^{-6}	7.85×10^{-1}	2.02×10^{-5}	5.37×10^{-1}

4. Conclusion

Corrosion and microstructural properties of TiO_2–CeO_2 composite films prepared by sol–gel method and heat treated at 300, 400, and 500 °C have been investigated. XRD patterns revealed a completely amorphous structure of the sample heat treated at 300 and 400 °C. Structure of TiO_2–CeO_2 thin films heat treated at 500 °C was crystalline and exhibited small amounts of crystalline phase corresponding to CeO_2. The absence of TiO_2 characteristic peaks confirms that crystalline CeO_2 phase is dispersed in an amorphous phase of TiO_2. The average grain size was approximately 22 nm. Electrochemical studies showed that by increasing the heat treatment temperature from 300 to 500 °C, the corrosion resistance of the films decreased. This lower corrosion resistance is attributed to crystallization of CeO_2 phase in TiO_2–CeO_2 composite films at higher sintering temperatures and consequent reduction in its ion and electrical conductance. Another explanation is that crystallization of CeO_2 leads to formation of fissures in the amorphous TiO_2 matrix which reduces the corrosion resistance of the coating. Corrosion current density of the film sintered at 300 °C was found to be 140 nA/cm^2 and this sample exhibited the best corrosion resistance as well. High resistance and low capacitance values of this film also confirmed its superior corrosion resistance.

References

[1] D. Wang, G.P. Bierwagen, Prog. Org. Coat. 64 (2009) 327–338.
[2] G. Carbajal, A. Martinez-Villafane, F.G. Gonzalez-Rodriguez, Anti-Corros. Method Mater. 4 (2001) 241.
[3] A.S. Hamdy, D.P. Butt, Surf. Coat. Technol. 201 (2006) 401–407.
[4] H. Yun, J. Li, H. Chen, Ch. Lin, Electrochim. Acta 52 (2007) 6679–6685.
[5] A. Balamurugan, S. Kannan, S. Rajeswari, Mater. Lett. 59 (2005) 3138–3143.
[6] P. Kern, P. Schwaller, J. Michler, Thin Solid Films 494 (2006) 279–286.
[7] G.X. Shen, Y.C. Chen, C.J. Lin, Thin Solid Films 489 (2005) 130–136.
[8] B.Y. Johnson, J. Edington, A. Williams, M.J. O'Keefe, Mater. Charact. 54 (2005) 41–48.
[9] B.Y. Johnson, J. Edington, M.J. O'Keefe, Mater. Sci. Eng. A361 (2003) 225–231.
[10] S. Nagarajan, N. Rajendran, Appl. Surf. Sci. 255 (2009) 3927–3932.
[11] Ch. Jing, X. Zhao, Y. Zhang, Mat., Sol–gel fabrication of compact, crack-free alumina film Res. Bull. 42 (2007) 600-608.
[12] A. Verma, D.P. Singh, A.K. Bakhshi, S.A. Agnihotry, J. Non-Cryst. Solids 351 (2005) 2501–2512.
[13] A. Verma, A.K. Bakhshi, S.A. Agnihotry, Electrochim. Acta 51 (2006) 4639–4648.
[14] M. Bethencourt, F.J. Botana, J.J. Calvino, M. Marcos, M.A. Rodriguez Chacon, Corros. Sci. 39 (1998) 1803–1819.
[15] S. Palmas, F. Ferrara, M. Mascia, A.M. Polcaro, J.R. Ruiz, A. Vacca, G. Piccaluga, Int. J. Hydrogen Energy 34 (2009) 1647–1654.
[16] H. Wang, R. Akid, Corros. Sci. 49 (2007) 4491–4504.